A Modular, Smart, and Wearable System for High Density sEMG Detection

This article has been accepted for publication in a future issue of this journal, but has not been fully edited. Content may change prior to final publication. Citation information: DOI 10.1109/TBME.2019.2904398, IEEE Transactions on Biomedical Engineering

A Modular, Smart, and Wearable System for High Density sEMG Detection

Giacinto Luigi Cerone*, *Member, IEEE*, Alberto Botter, and Marco Gazzoni

Abstract — Objective: **The use of linear or bi-dimensional electrode arrays for surface EMG detection (HD-sEMG) is gaining attention as it increases the amount and reliability of information extracted from surface EMG. However, the complexity of the setup and the encumbrance of HD-sEMG hardware currently limits its use in dynamic conditions. The aim of this work was to develop a miniaturized, wireless, and modular HD-sEMG acquisition system for applications requiring high portability and robustness to movement artifacts.** ***Methods:*** **A system with modular architecture was designed. Its core is a miniaturized 32-channel amplifier (Sensor Unit - SU) sampling at 2048sps/ch with 16bit resolution and wirelessly transmitting data to a PC or a mobile device. Each SU is a node of a Body Sensor Network for the synchronous signal acquisition from different muscles.** ***Results:*** **A prototype with two SUs was developed and tested. Each SU is small (3.4cm x 3cm x 1.5cm), light (16.7g), and can be connected directly to the electrodes thus avoiding the need for customary, wired setup. It allows to detect HD-sEMG signals with an average noise of 1.8μV$_{RMS}$ and high performance in terms of rejection of power-line interference and motion artefacts. Tests performed on two SUs showed no data loss in a 22m range and a ±500μs maximum synchronization delay.** ***Conclusions:*** **Data collected in a wide spectrum of experimental conditions confirmed the functionality of the designed architecture and the quality of the acquired signals.** ***Significance*****: By simplifying the experimental setup, reducing the hardware encumbrance, and improving signal quality during dynamic contractions, the developed system opens new perspectives in the use of HD-sEMG in applied and clinical settings.**

***Index Terms*— Body Sensors Networks, Dynamic EMG, HD-sEMG amplifier, Modular systems, Movement artefacts, Smart devices, Wearable sensors.**

I. Introduction

CURRENTLY, the detection of surface electromyograms (sEMGs) in applied studies is mainly based on single electrode pairs positioned over individual muscles (bipolar sEMG detection) with the purpose of: (i) estimating the degree and timing of muscle activation, (ii) providing biofeedback on the level of muscle activity, (iii) estimating muscle force, (iv) controlling a prosthesis, a robot, or some artificial device. However, in the last two decades limitations of bipolar sEMG emerged. Bipolar sEMG provides a global indication on the degree of muscle activity which may or may not be sufficiently informative, depending on the aim of the measure. Global features extracted from a single, bipolar sEMG are influenced by both central and peripheral properties of the neuromuscular system [1], [2], whose contribution cannot be discriminated. Moreover, a single bipolar sEMG provides a local sampling of muscle activity while a growing number of works in literature report regional patterns of muscle activation and heterogeneous sEMG activity during voluntary and electrically-induced contractions [3]–[7]. Therefore, the accuracy of muscle activation estimates based on bipolar sEMG depends on muscle size, structure, and function as well as on the electrode positioning and inter-electrode distance [4], [7]–[9]. Being able to sample the distribution of sEMG with an appropriate spatial sampling has been proven to be crucial in several applications [10], [11]. The above considerations become more critical in dynamic conditions because of the continuous modifications in the force output, muscle fiber length, and relative position of surface electrodes and EMG sources [12].

Systems based on multiple electrodes arranged in linear arrays or bi-dimensional grids covering the muscle surface have been proposed to increase the amount and reliability of information extracted from sEMG, [11], [13]–[21].This technology, also referred to as High-Density surface EMG (HD-sEMG), allows for the extraction of anatomical and physiological information either at the muscle or at the motor unit level [15], [22]–[28] with applications in several fields ranging from neuromuscular physiology [29]–[33] to clinical neurophysiology [34]–[40], and control of prosthetic devices [41]–[46].

Even though HD-sEMG opened new perspectives in neuromuscular assessment, several challenges related to signal detection and interpretation are still open, especially in dynamic conditions. Few portable HD-sEMG amplifiers have been proposed in the literature: Pozzo et al. proposed a 64 channel sEMG datalogger [47]; Barone and Merletti described a 64 channel sEMG amplifier with optical cable connection for data transmission [48], and some portable devices with wireless connection between a control unit on the subject and the laptop are available on the market. However, the size and weight of such devices together with the presence of cable connections between the arrays/grids of electrodes and the amplifier, pose important limitations for dynamic HD-sEMG recordings. Issues like system encumbrance, setup complexity, movement limitation imposed by the cables, movement artefacts affecting the signals are indeed the main bottleneck limiting the use of HD-sEMG technique in applied scenarios.

This research was supported by the bank foundation "*Compagnia di San Paolo", Torino, Italy.*

*G.L. Cerone, A. Botter. And M. Gazzoni are with the Laboratory for Engineering of the Neuromuscular System (LISiN), Dipartimento di Elettronica e Telecomunicazioni, Politecnico di Torino, Italy (Correspondence e-mail: giacintoluigi.cerone@polito.it).

This article has been accepted for publication in a future issue of this journal, but has not been fully edited. Content may change prior to final publication. Citation information: DOI 10.1109/TBME.2019.2904398, IEEE Transactions on Biomedical Engineering

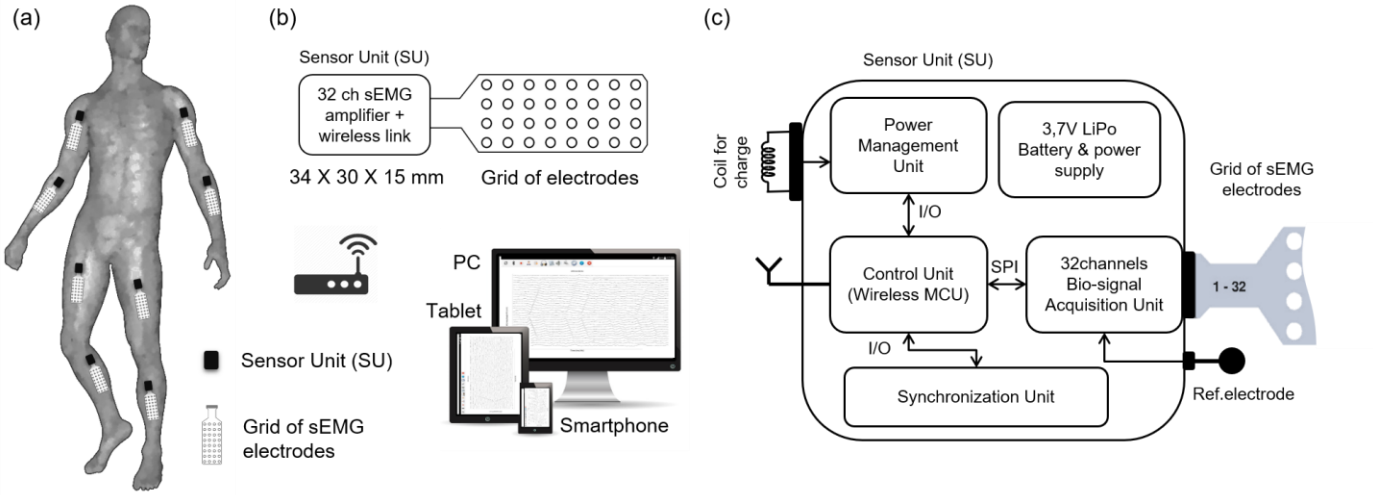

Fig. 1. System architecture. (a) Electrode arrays or grids are applied on the skin over the muscles under investigation. Each detection system is connected to one Sensor Unit (SU) performing the conditioning, sampling and wireless transmission of 32 monopolar sEMG channels sampled at 2048sps with 16-bit resolution. (b) Each SU transmits the acquired signals to either a mobile device (smartphone or tablet with Wi-Fi connectivity) or a Personal Computer for real-time visualization and storage. (c) Block diagram of the SU. The Bio-signal Acquisition Unit implements the conditioning and sampling of 32 monopolar sEMG signals. The Control Unit is a wireless MCU integrating a Main Processor (MP) and a Network Processor (NWP) running in parallel. The MP configures and controls the Bio-signal Acquisition Unit and organizes the acquired data in packets. The NWP manages the Wi-Fi connection and sends the sampled data wirelessly to the receiver. The Power Management Unit provides a regulated 3.3V power supply and handles the battery charging process. The Synchronization Unit implements the synchronization between more SUs.

We identified the following requirements for a new HD-sEMG acquisition system overcoming the current limitations.

Modular architecture: since in the study of dynamic contractions more than one muscle is usually monitored, a modular, wireless architecture able to manage the data throughput from a set of acquisition modules positioned over different muscles is required.

Reduction of the size and weight of the device: miniaturized electronics allows to integrate the conditioning circuitry near the electrodes, thus avoiding connecting cables between the detection and conditioning systems. This would improve the portability of the system, simplify the experimental setup, and reduce the susceptibility to motion artifacts.

Mobile interface: The interface with mobile devices may improve the usability of the system, a relevant aspect in applied scenarios. Moreover, interfacing with mobile devices would allow obtaining a virtually unlimited field of measure by streaming the data over the Internet.

The aim of this work was to develop a miniaturized, wireless, and modular HD-sEMG acquisition system directly interfacing with laptops, smartphones or tablets, as a tool for enabling new research frontiers in the non-invasive analysis of neuromuscular system. To the best of our knowledge such a system for HD-sEMG is not available on the market and has not been described in the literature.

II. System Design

A. General Architecture

Fig. 1 shows the general architecture of the developed system. The core of the system is a wireless miniaturized 32-channel sEMG amplifier (Sensor Unit - SU) that can be used as a node of a Body Sensor Network (BSN) for the monitoring of different muscles. Each SU performs the conditioning, sampling, and wireless transmission of 32 monopolar sEMG channels, sampled at 2048ksps with 16bit resolution. The SU wirelessly transmits the acquired signals to either a mobile device or a personal computer for real-time visualization and storage. Signals are transmitted to the receiver with two modalities: (i) via direct link (point-to-point connection), when only one SU is used or (ii) through an access point acting as a router, when more than one SU is used. Each SU acts as a client while the receiver acts as a Server.

B. Sensor Unit Design

Table I shows the characteristics of the SU module. The SU consists of four main building blocks (Fig. 1.c): 1) the Bio-signal Acquisition Unit, 2) the Control Unit (CU), 3) the Power Management Unit and 4) the Synchronization Unit.
The detailed description of each block is reported in the following.

1) Bio-signal Acquisition Unit

The Bio-signal Acquisition Unit implements the conditioning, sampling, and quantization of 32 sEMG signals. The following requirements were considered for the analog front-end selection: 1) device miniaturization in order to minimize the size and encumbrance of the system and consequently, to improve the robustness to movement artefacts; 2) possibility to acquire at least 32 channels; 3) detection of sEMG signals in monopolar configuration to maximize the informative content of the recorded signals; 4) availability as pre-packaged component for standard pick and place mounting of the PCB.

This article has been accepted for publication in a future issue of this journal, but has not been fully edited. Content may change prior to final publication. Citation information: DOI 10.1109/TBME.2019.2904398, IEEE Transactions on Biomedical Engineering

TABLE I. SENSOR UNIT TECHNICAL SPECIFICATIONS

Description	Parameter	Value
Number of channels	N	32
EMG Bandwidth	BW_{EMG}	10 Hz – 500 Hz
Gain	G	192 ± 1 V/V
Common Mode Rejection Ratio	CMRR	82 dB
Input Impedance module	$\|Z_{In}\|$	1,3 GΩ (10 Hz) 13 MΩ (1 kHz)
Input Range	IR	10 mV_{pp}
RTI Noise	N_{RTI}	< 3 μV_{RMS}
A/D Resolution	Res	16 bit
Sampling Frequency	f_s	2048 sps
Communication	-------	Wi-Fi
Receiver Type	-------	PC, Smartphone or Tablet
Max. Synchronization delay	Δt_{Sync}	±500 µs
Max. transmission distance	d_{TX}	22 m (<0,02% data loss)
Power Supply	-------	600 mAh 1-Cell LiPo Battery
Life time (transmitting)	T_{TX}	5h
Dimensions	-------	3,4cm x 3cm x 1,5cm
Weight	-------	16,7g

Based on these requirements, we identified the Intan RHD2132 chip [49], [50] (Intan Technologies, California, USA) as the most suitable solution. This chip is a low-power and ultra-compact (size 9x9mm) bio-signal acquisition system, integrating 32 monopolar AC-coupled analog front-ends with fixed gain (192V/V) and programmable bandwidth (0.1Hz – 20kHz), three non-conditioned auxiliary channels, a 35-channel analog multiplexer, a 16-bit successive-approximation-register (SAR) A/D converter and a SPI communication interface.

Although some of the characteristics of RHD2132 chip are below the state of the art for a bio-signals amplifier (e.g. CMRR=82dB, input impedance ≈1GΩ at 50Hz) the overall features of the front-end may be adequate for the acquisition of sEMG signals. Indeed, for miniaturized systems with floating, battery powered supply, the stray capacitance between the amplifier's reference and the power line ground is in the range of few tens of picofarad [51]. Considering that the capacitive coupling between the subject and the power line is limited below few volts RMS, the common mode voltage at the input of the analog front-end (V_{CIN}) can vary between few to few tens of millivolts [51]–[53]. If we consider a maximum impedance unbalance of few hundreds of kiloOhms [54], the input-referred power line interference of RHD2132 chip is about 10µV_{RMS} in the worst-case scenario (i.e. V_{CIN}=125mV_{RMS}) [55]. Therefore, the overall characteristics of Intan RHD2132 in terms of miniaturization, number of channels, and also rejection of power line interference (when used in ground-floating systems), are adequate for the aims of this study.

2) Control Unit

The Control Unit implements the sampling and wireless transmission of the signals. Sampling 32 signals at 2048sps with 16-bit resolution requires a constant data throughput of 1Mbps. Several wireless communication protocols offer the possibility to create Wireless Sensor Networks (WSN) and allow to obtain the required data throughput. Among these, Wi-Fi supports high data rate, TCP(UDP)/IP internet protocol stack and allows the communication with both mobile devices and PCs. The main drawback of the Wi-Fi technology is power consumption. Bluetooth is less power consuming, however, it is limited in terms of throughput and does not allow the connection of more than 7 nodes to the network. Zigbee and 6LowPan offer the advantages of Wi-Fi with lower power consumption but require the use of a PC as a receiver and are not natively supported by mobile devices.

The choice of using a wireless protocol natively supported by mobile devices, which excludes the possibility of using a PC configured as a "bridge", is because we aimed at developing a completely wearable system. Indeed, this solution allows wearing also the receiver, thus enabling the possibility to use the system in outdoor scenarios without the burden of an additional, custom-made receiver.

In order to achieve the required data throughput and to allow the connection of multiple SUs to mobile devices without an ad-hoc receiver, we opted for the Wi-Fi transmission protocol and selected the Texas Instruments CC3200 system-on-chip wireless MCU. The CC3200 integrates an ARM Cortex-M4 MCU core (Main Processor, MP) running at 80MHz and an additional dedicated ARM MCU (Network Processor, NWP) that acts as a Wi-Fi network processor subsystem including an embedded TCP/IP stack. The NWP manages the Transport (TCP), Network (IP) and Physical layers of the TCP/IP model applied to the Wi-Fi protocol and uses a standard BSD Socket implementation as Application Programming Interface (API). This feature allows limiting the tasks performed by MP to 1) data sampling and 2) management of the application layer of the transmission protocol.

Two tasks, the Sampling Task (managed by MP) and the Transmission Task (managed by NWP) run in parallel on the FreeRTOS Real Time Operating System embedded into the CC3200 device. The Sampling Task communicates with the Intan RHD2132 chip through the SPI peripheral (20MHz clock frequency) and stores the sampled data in a circular buffer. The communication between the RHD2132 and the CC3200 SPI Peripheral is managed by the DMA (Direct Memory Access) peripheral embedded into the CC3200. When 22 samples per channel are available in the circular buffer, the MP creates a new data packet and instructs the NWP to add it to the payload. The data packet is composed by 702 WORDs containing the sampled data interlaced (20 samples x 32 channels) and terminates with four bytes: SysID, ProbeID, Ramp, and Check. The SysID byte is the unique identifier of the body network, ProbeID identifies the SU into the network and Ramp is an incremental counter used to detect packet losses. The Check byte contains a standard CRC-8 checksum used to identify corrupted packets.

The NWP integrates the Network Stack (IP Layer and TCP Protocol) and the mDNS (multicast DNS) Service Discovery protocol for the automatic connection with unknown IP addresses. These features allow offloading the MP from all the operations needed to start a connection with a server, send/receive data, and managing the protocols implementing the Physical (MAC), the Internet (IP), and the Transport (TCP) layers. When a new payload is available, the MP instructs the

This article has been accepted for publication in a future issue of this journal, but has not been fully edited. Content may change prior to final publication. Citation information: DOI 10.1109/TBME.2019.2904398, IEEE Transactions on Biomedical Engineering

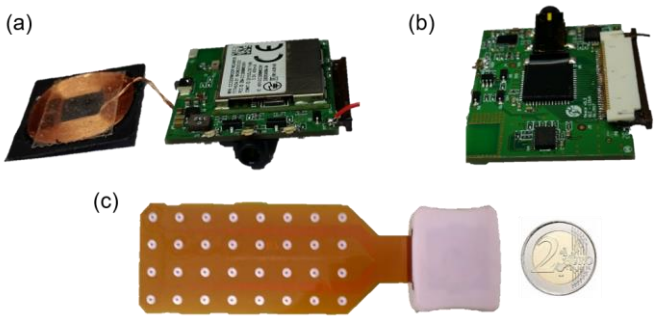

Fig. 2. Sensor Unit (SU) Prototype. The eight layers, 1mm thick PCB with mounted components is shown in (a) and (b). The PCB's top side hosts the CC3200 MCU, the power supply circuitry, the On/Off pushbutton, the programming connector and three LEDs indicators. The PCB's bottom side hosts the RHD2132 chip, the battery charging circuit with the relative coil and the synchronization unit are mounted. The PCB dimensions are 30mm x 25mm x 1mm. (c) SU module enclosed in a 3D printed PLA case and connected to a flexible Kapton® grid of 32 Ag electrodes. The total encumbrance of the SU is 3.4cm x 3cm x 1.5cm.

NWP to send it to the server over the TCP/IP Layer.

In order to identify the optimal payload length to satisfy the required data throughput we varied the number of data packets into the payload between 1 and 1000. The Wi-Fi data throughput has been analyzed by means of the Open Source Wireshark Wi-Fi packet sniffer software and calculated as in Eq. (1).

$$Throughput = \frac{T_{TX}}{N_{RX} * 1000} \qquad (1)$$

where the throughput is expressed in kbps while T_{TX} and N_{RX} are the acquisition time in seconds (fixed to 5 minutes) and the number of received bits respectively.

Since MP and NWP share the same RAM, a 10 payloads long circular buffer has been used to avoid conflicts between the Sampling and the Transmission tasks. The two tasks are synchronized to avoid the Transmission task, which is asynchronous and non-blocking, is executed when no new data are available. Indeed, a single interrupt routine performing data sampling, payload organization, and transmission would lock the system for a period greater than the sampling interval (500µs), thus resulting in loss of samples. Therefore, the Sampling and the Transmission tasks were synchronized using a binary semaphore. The semaphore is locked by the Sampling Task until a new data packet is available, then the semaphore is released. The Transmission Task attempts to "take" the semaphore and if this is not available it remains locked. When the Sampling Task changes the semaphore status, the transmission task executes the data sending process through the NWP processor.

3) Power Management Unit

The Power Management Unit provides a regulated 3.3V power supply and handles the wireless battery charging process. The system is powered through a 600mAh single-Cell LiPo Battery while the 3.3V regulated power supply voltage is obtained through a Texas Instruments TPS62172 synchronous, stepdown DC-DC converter with an efficiency higher than 90% and a maximum output current of 500mA.

Charging the system wirelessly provides galvanic isolation between the battery-powered SU and the non-isolated charging base, thus reducing the risk of unwanted leakage current flowing between the battery charging circuit and other devices connected to the patients.

The battery is charged through the BQ24232 chip (Texas Instruments, Texas, USA) embedded in the system. The BQ24232 chip integrates a Dynamic Power-Path Management (DPPM) system that powers the device while simultaneously and independently charges the battery. This feature is needed to reduce the charging time considering the SUs are synchronized when in charge (for details refer to section II.4 - Synchronization Unit). The 5V power supply needed to charge the battery is obtained through the P9027LP-R wireless power receiver (IDT, California, USA). The P9235A-R-EVK evaluation board was used as wireless charger transmitter and powered from an USB 2.0 port.

The system was equipped with a 2W coil as a compromise choice between battery charging time, coil's encumbrance, and efficiency of the wireless power transfer (>90%).

4) Synchronization Unit

When two or more SUs are used at the same time as a wireless BSN, the data sampling must be synchronous among the SUs. The Synchronization Unit implements the synchronization between two or more SUs.

The SUs synchronization is obtained by providing the SUs with a common pulse signal triggering the start of the Sampling task. The ACT pin of the P9027A-R chip was used as trigger source to reduce the number of components and consequently the overall size of the system. The ACT pin is an open drain output that pulls down when the connection between the wireless power receiver and transmitter is established. The Sampling Task starts simultaneously on all SUs when the trigger signal is received.

5) System Prototype

The SU design was kept as simple as possible using only Commercially-available Off-The-Shelf (COTS) components. The minimization of system's encumbrance was one of the primary objectives of the design. Molex 54104-3231 (21.5mm x 1.8mm) connector was chosen for the connection with a flexible Kapton® grid of 32 Ag electrodes.

The reference electrode is connected to the system through a short cable (Fig. 3b). Fig. 2 shows the prototype of one SU. It consists of an eight-layers, 1mm thick PCB (dimensions: 3cm x 2.5cm) with components mounted on both sides. The top side (Fig. 2.a) hosts the CC3200 MCU, the power supply circuitry, the On/Off push button, the programming connector and three LEDs indicators. The PCB bottom side (Fig. 2.b) mounts the RHD2132 chip, the Synchronization and the Power Management units.

Two SU prototypes have been mounted and encapsulated in a 3D printed case (Fig. 2.c). The total encumbrance of the system (one SU) is 3.4cm x 3cm x 1.5cm.

This article has been accepted for publication in a future issue of this journal, but has not been fully edited. Content may change prior to final publication. Citation information: DOI 10.1109/TBME.2019.2904398, IEEE Transactions on Biomedical Engineering

C. Software

A standalone software was developed for the acquisition and online visualization of the sEMG signals on the receiver. The software was developed using the C++ multi-platform Qt libraries (Android, Windows, Linux and MAC). At the startup, the software initializes a TCP server and creates a TCP socket for each connected SU. The software uses the Zero Configuration Network (Zeroconf) protocol to provide the SU with the IP address of the server IP address without a priori information.

III. System Characterization

A. Bio-signal Acquisition Unit

The input-referred noise level of the front-end amplifier was measured by shorting and connecting to the reference pin the analog inputs of the RHD2132 chip. RMS voltage for each channel was calculated on 30s of signal.

The mean noise level across channels was 1.8±0.2μV_{RMS}. This value is comparable with the input-referred noise levels declared by most of commercially-available HD-sEMG systems, which are in the range 1μV_{RMS} - 10μV_{RMS}, depending on the device. The 0.2μV_{RMS} discrepancy between this result and the typical value declared in the datasheet of RHD2132 (2.0 μV_{RMS}) may be associated with the relatively small sample we used for noise measures (64 channels). A larger number of prototypes must be characterized in order to compare our findings with the typical value reported in RHD2132 datasheet.

The band-pass gain of each channel was measured by applying a 80Hz, 2mVpp sinewave to the input of the RHD2132 front-end and calculating the ratio between the output and the input peak-to-peak amplitude. The bandwidth of each monopolar front-end was measured by applying a 2mVpp sinewave to the input and varying the input frequency in order to find frequency values corresponding to -3dB attenuation with respect to the nominal gain of each channel. The measured in-band gain for each channel was 192±1V/V (CoV = 0.5%) within a 10Hz - 500Hz frequency band. The measured inter-channel gain variability was comparable with that declared by commercially available HD-sEMG amplifiers, ranging between 0.5% and 1%. All the channels had a minimum measured input voltage range of 10mV_{pp} (±5mV_{pp}).

The Total Harmonic Distortion (THD) was calculated in the 10 Hz - 500 Hz frequency band for three sinusoids of different amplitude (2mV_{pp}, 4mV_{pp}, and 8mV_{pp}). The measured THD was less than 0.8% in the bandwidth of interest, in agreement with the values reported in the RHD2132 datasheet. The considered mid-band frequencies (80Hz and 280Hz) showed a THD lower than 0.2%.

The robustness of the Bio-signal Acquisition Unit to the second-order non linearities introduced by the linear combination of two similar tones (amplitude 2mV_{pp}) at 99Hz and 101Hz was evaluated. The first-order IMD products, located at 97Hz and 103Hz were attenuated of 79.1dB±2.4dB with respect to the input signals.

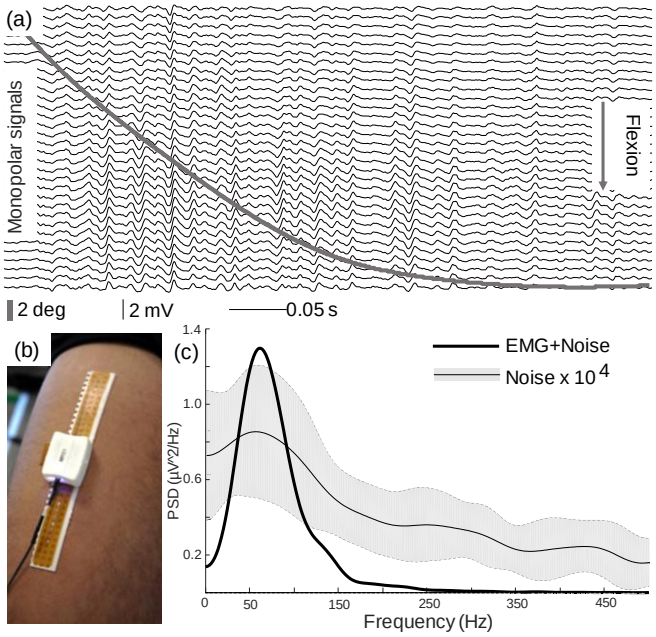

Fig. 3. (a) Monopolar sEMG signals recorded during knee extension from rectus femoris. The superimposed gray line is the knee joint angle. Signals were detected using a linear electrode array (32 electrodes, 5 mm inter-electrode distance) and one SU connected directly (without cables) to the electrode array positioned over the rectus femoris (b). The black cable connects the SU with the reference electrode positioned over the patella. (c) Mean Power Spectrum Density (PSD) estimated over all the channels (1Hz spectral resolution, Welch's method over 20 windows). It is possible to observe the absence of spikes at the power line frequency (50Hz). The PSD of the noise (mean and standard deviation are shown) is four orders of magnitude lower than the EMG signals over the entire EMG spectrum and shows the typical behavior of the flicker noise.

B. Wi-Fi link performance

The data throughput was estimated by varying the number of packets for each data frame using: 1) a single task for sampling and transmission and 2) two different tasks, synchronized using a binary semaphore for the sampling and transmission processes. The use of two different tasks speeds-up the data-throughput because in this way there are no conflicts between the sampling and sending tasks. Moreover, the transmission task can be completely managed through the NWP of the CC3200 chip, resulting in a non-blocking process. The improvement obtained by increasing from 1 to 10000 data packets per frame (using semaphores) was about 40%. The maximum throughput of 9Mbps was obtained with 10000 data packets per frame, allowing the transmission of up to 282 sEMG channels sampled at 2048ksps with 16-bit resolution. However, such a data frame size (corresponding to 55s) is not compatible with the online visualization of the signals. Nevertheless, the data throughput obtained with 1 data packet (10ms) per frame was 5.5 Mbps. This means that each SU could theoretically transmit up to 170 sEMG channels (2048sps, 16-bit resolution).

Although the upper-bound is 170 channels, we used a single RHD2132 chip (32 channels) per SU as a compromise between the number of channels for each SU and the SU miniaturization. Our system allows to acquire more than 32 sEMG signals using several SUs at the same time. In this case the total data

This article has been accepted for publication in a future issue of this journal, but has not been fully edited. Content may change prior to final publication. Citation information: DOI 10.1109/TBME.2019.2904398, IEEE Transactions on Biomedical Engineering

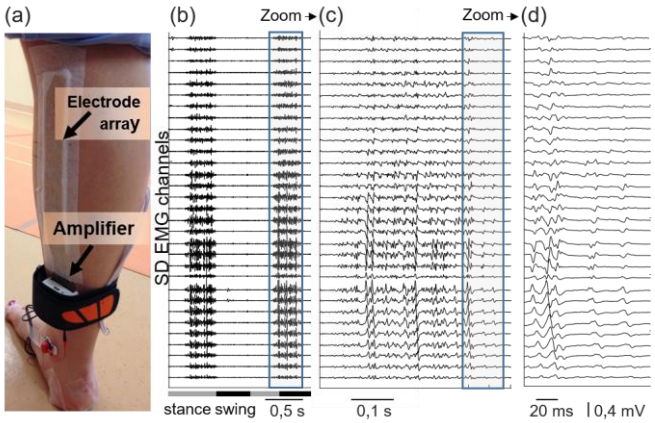

Fig. 4. Example of signals acquired from a single SU module during gait. (a) A linear array with 32 electrodes and inter-electrode distance of 5 mm was positioned on the medial gastrocnemius covering the whole length of the muscle. (b) SD signals recorded during two steps. It is possible to observe the good quality of the signals and the absence of movement artefacts. (c) Zoom showing the sEMG activity burst during the second step. (d) Zoom on the end of the signal epoch shown in (c). MUAP propagation is clear in the distal portion of the muscle.

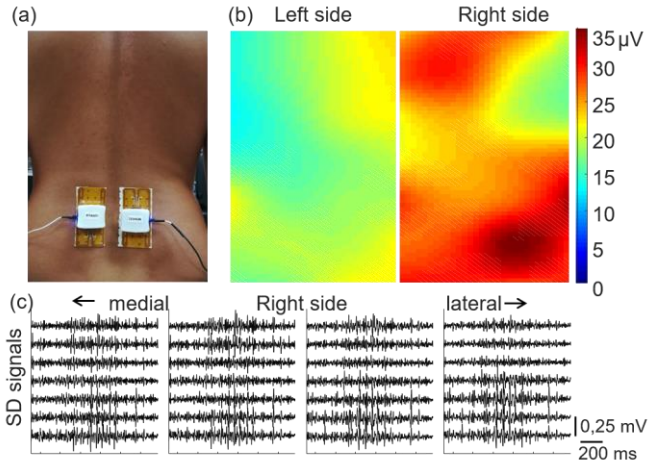

Fig. 5. Example of HD-sEMG acquisitions from back muscles during a lifting task. (a) Experimental setup. Two grids of electrodes (8x4 electrodes, inter-electrode distance: 10 mm) were positioned bilaterally over the lumbar muscles. Two synchronized SUs were used to acquire the signals. (b) sEMG distribution (RMS maps interpolated by a factor 10) during one repetition of the task for the left and right side. (c) Single differential signals detected from the right side during one repetition of the task and used to calculate the sEMG distribution reported in b).

throughput increases, but the data throughput of each SU remains the same.

The latency of the wireless link was measured by feeding a common trigger signal to our system and to a reference, cabled, acquisition system with latency lower than 100µs used as gold standard (Quattrocento, OT Bioelettronica, Torino, Italy). A Matlab script was used to start the acquisition of the two signals simultaneously and the latency was than measured offline. The average latency was 12ms±2ms.

The TCP packet loss was measured by means of the Wireshark network analyzer software during five-minute acquisitions at different transmitter-receiver distances. The maximum transmission distance was identified as that ensuring a packet loss <0.02%. This distance was 22m outdoor. The average packet loss in this condition was 0.016%, corresponding to 48ms out of 300s. A direct comparison with commercially available systems for HD-sEMG recording was not possible because these information (transmission distance and data loss) are not disclosed by the Manufacturers.

C. *Synchronization*

Synchronization tests were performed with two SUs by applying a 80Hz, 2mVpp sinewave as a common input and recording 30s of signal. The acquisition was repeated 8 times. The time delay between the signal recorded on the first channel of the SUs was computed using the cross-correlation between the channels. The maximum time misalignment between two SUs was within ±500µs (i.e. ±one sample). The same result was obtained for the delay between the signals transmitted by two SUs after a one-hour long acquisition, showing no significant drift in time due to the different clock sources.

D. *Current Consumption*

The system is powered by a 1-cell LiPo battery with capacity of 600mAh. The measured current consumption during continuous transmission was 119 mA. The system allowed continuous acquisition for up to 5 hours in accordance with the expected performance. The time required to recharge completely the SU module was two hours.

E. *Experimental Tests*

The developed system was field tested in a wide spectrum of conditions ranging from slow to fast dynamic tasks. These experiments were devised to demonstrate the feasibility of HD-sEMG detection in experimental conditions for which such acquisitions would be highly challenging due to either the setup complexity (i.e. number of sampled muscles) or the possible occurrence of movement artifacts.

1) *Leg Extension Exercises*

HD-sEMG signals were acquired during knee extension using a leg extension machine.

Fig. 3.b shows the experimental setup. The subject sat on a leg extension machine (Panatta, Apiro, Italy) set for a range of motion between 80º and 170º (where 180º corresponds to knee maximum extension).

Surface EMG signals were recorded from the right rectus femoris using a linear electrode array (32 electrodes, 5 mm inter-electrode distance) and from the right vastus medialis muscle using an 8 x 4 electrode grid, with 5 mm inter-electrode distance.

Fig. 3.a shows one representative epoch of monopolar sEMG signals (0.5s) recorded from the rectus femoris. Fig. 3.c shows the mean Power Spectrum Density (PSD) estimated over the 32 channels (1Hz spectral resolution, Welch's method over 20 windows). Both in the time-domain signals and in the power spectral density it is possible to observe the absence of power line interference. This is an expected result, considering the features of the selected front-end and the fact that the system is floating with respect to the ground potential (see section II.B) [11], [51]–[53]. The PSD of the noise was four order of magnitude lower than the sEMG signals over the whole sEMG

This article has been accepted for publication in a future issue of this journal, but has not been fully edited. Content may change prior to final publication. Citation information: DOI 10.1109/TBME.2019.2904398, IEEE Transactions on Biomedical Engineering

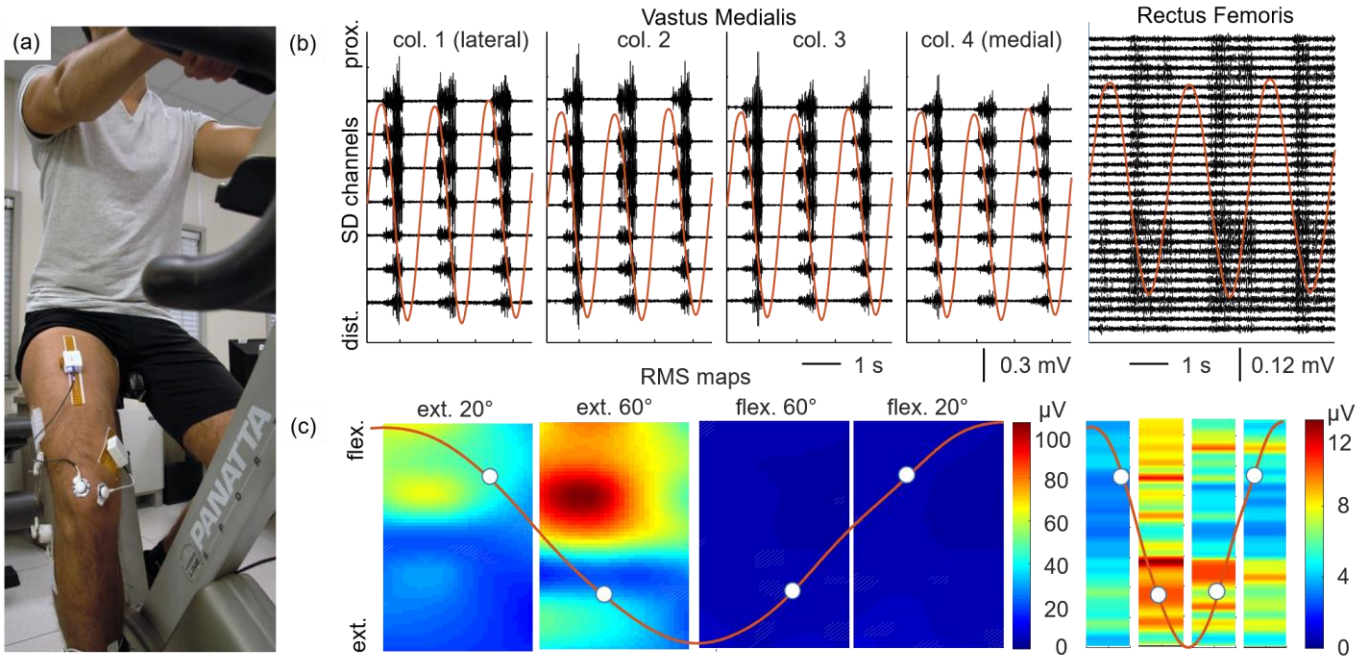

Fig. 6. Test of the system during a cycling task at 30 rpm. (a) Two SUs were used, one connected to a 8x4 grid of electrodes (inter-electrode distance: 10mm) positioned over the vastus medialis muscle and one connected to a 32 electrodes linear array (inter-electrode distance: 5 mm) positioned over the rectus femoris muscle. The knee-joint angle was acquired by means of an electro-goniometer. (b) SD signals recorded during three cycles are shown superimposed with the knee angle for both vastus medialis and rectus femoris muscles. The quality of the signals is good and movement artefacts are absent. (c) RMS maps calculated on 125ms-long epochs centered in correspondence of four phases of the cycling (20° and 60° of knee angle (full extension: 0°) during both flexion and extension). Vastus medialis is active during the knee extension while the rectus femoris is active during the whole cycle, acting as knee extensor and hip flexor.

spectrum.

2) Gait

The developed system was tested for the acquisition of HD-sEMG signals during gait. Fig. 4.a shows the experimental setup. A linear array of 32 electrodes and inter-electrode distance of 5 mm was positioned on the medial gastrocnemius muscle covering the whole length of the muscle. Two footswitches were placed under the heel and the big toe for gait event detection. Auxiliary signals provided by the footswitches were recorded synchronously with sEMG signals through a system for biomechanical signal acquisition (DueBio, OTBioelettronica, Italy). HD-sEMG signals were recorded in monopolar configuration while the subject was walking along a straight, 12m long path at spontaneous speed. Single differential (SD) signals were computed via software as the difference between consecutive monopolar channels. From the SD signals (Fig. 4.b) it is possible to identify muscle activation bursts without the presence of movement artefacts and the propagation of MUAPs in the distal region of the muscle [56].

3) Lifting Task

This task was aimed at simulating a work-related activity. The subject was asked to repetitively move a load (weight: 5kg) between 2 shelves placed at knee and hip height. HD-sEMG signals were acquired bilaterally from lumbar erector spinae muscle using two grids of electrodes (8x4 electrodes, inter-electrode distance: 10 mm) (Fig. 5.a). During this slow dynamic task (1 cycle/2 s) signals were stable without movement artefacts (Fig. 5.c). The sEMG root mean square (RMS) value was computed for each location of the grid to generate a colour map representing the sEMG amplitude distribution (Fig. 5.b). From the RMS maps it is possible to study the differences in the muscle activity between sides and changes in time as shown in [57].

4) Cycling

HD-sEMG signals were recorded from rectus femoris and vastus medialis muscles during cycling at different speeds (30rpm and 60rpm). Signals were recorded from the rectus femoris using a linear electrode array (32 electrodes, 5 mm inter-electrode distance) and from vastus medialis using a grid of electrodes (8x4 electrode grid, 10mm inter-electrode distance). Signals were recorded in monopolar configuration and SD signals were computed via software. The cycling phases were identified based on the knee joint-angle detected by an electrogoniometer connected to a system for the acquisition of biomechanical signals (DueBio, OT Bioelettronica, Italy). An example of signals recorded during a cycling task at 30rpm is reported in Fig. 6. The high signal quality and the absence of movement artefacts allow the study of muscle activity distribution during all the cycling phases, as shown by the RMS maps in Fig. 6.c.

5) Jumping

In order to stress the performances of the developed system in dynamic conditions, HD-sEMG signals were recorded during vertical jumps with counter-movement (Fig. 7.b). sEMG signals (Fig. 7.a) were detected from vastus medialis muscle of the right leg using a grid of electrodes (8x4 electrodes, inter-electrode distance: 5 mm). Signals were recorded in monopolar

This article has been accepted for publication in a future issue of this journal, but has not been fully edited. Content may change prior to final publication. Citation information: DOI 10.1109/TBME.2019.2904398, IEEE Transactions on Biomedical Engineering

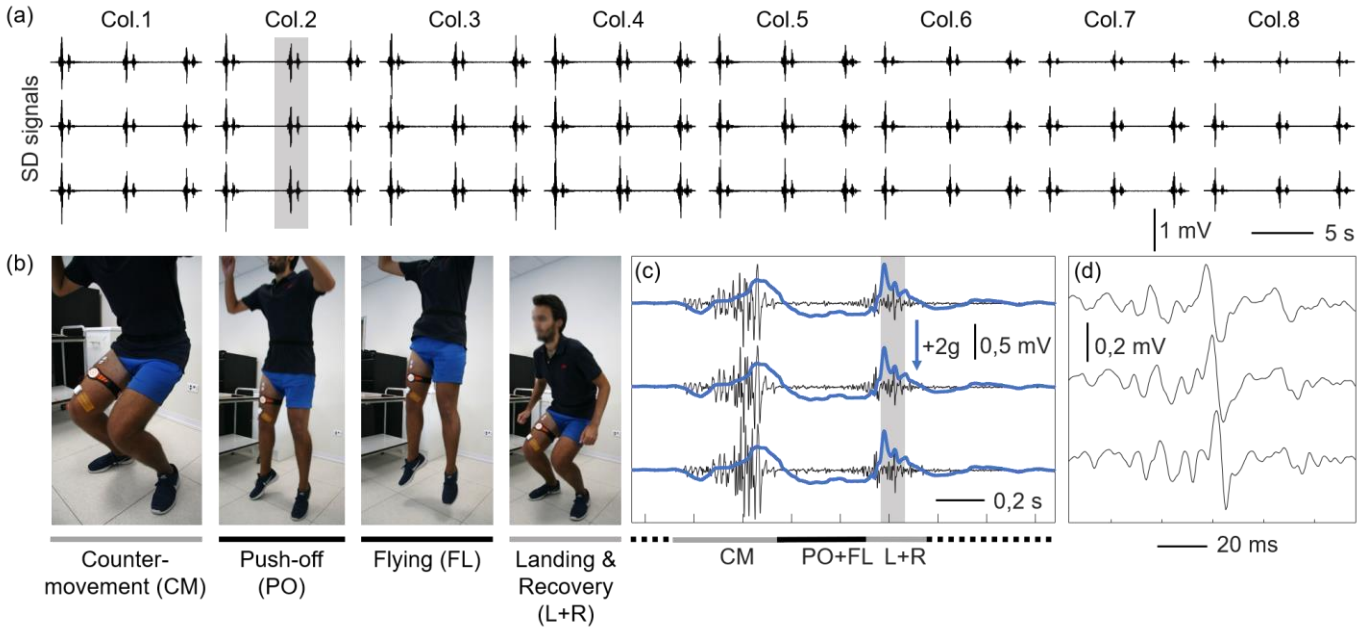

Fig. 7. Test of the system during a jumping task with counter movement. (a) Single differential (SD) signals recorded from vastus medialis during three jumps (4x8 grid of electrodes, inter-electrode distance: 10 mm). (b) Segmentation of the single jump in four phases. (c) Zoom showing the signals recorded from the second column of the grid during the second jump (the corresponding epoch is highlighted in (a)). Signals are shown superimposed with vertical acceleration profile (blue line) acquired by means of a single axis inertial sensor placed on the L5 vertebra. Movement artefacts are absent also in correspondence of the acceleration peak (landing and recovery phase). (d) Zoom on the signal epoch shown in (c) (gray box). It is possible to observe MUAP propagation.

configuration and SD signals computed via software. A single axis inertial sensor (DueBio, OT Bioelettronica, Italy) to identify the jump phases was placed on the L5 vertebra and synchronized with the sEMG system. The high signal quality is demonstrated by the absence of movement artefacts during the landing and recovery phases, corresponding to the acceleration peak (Fig. 7.c).

It was possible to observe motor unit action potential propagation along the channels during all task phases (Fig. 7.d).

IV. Conclusion

Wearable sEMG acquisition systems described in literature or commercially available usually consist of 8-16 pre-amplified bipolar sEMG probes that transmit raw signals to a receiver and are mainly targeted on traditional gait and movement analysis. In the last years, HD-sEMG opened new perspectives in the non-invasive assessment of neuromuscular system [30], but several challenges related to signal detection and acquisition are still open, especially in dynamic conditions.

The main current issues are the system encumbrance, the setup complexity, the limitations imposed by the presence of connecting cables, and the susceptibility to motion artifacts. Movement artefacts are mainly due to (1) changes in skin thickness during movement, (2) reciprocal movement at the gel-electrolyte skin interface and, (3) cable movements [58] Klinj and Kloprogge [59] showed that motion artifacts generated by the cable movements are due to the tribolelectric noise due to the friction and deformation of cable insulation acting as piezoelectric transducer. While the two first causes can be reduced by scrubbing the skin [60] and using Ag-AgCl electrodes [61], the integration of the conditioning electronics close to the detection system without the use of connecting cables has the potential to drastically reduce motion artifacts due to triboelectric noise.

This paper describes the development, characterization, and test of a modular and wearable system for HD-sEMG, designed to address the aforementioned challenges. The developed system has a modular architecture, where each module is a HD-sEMG amplifier that wirelessly transmits 32 raw sEMG signals.

Each module is compact (3.4cm x 3cm x 1.5cm), light (16.7 g), and directly connected to the grid of electrodes without the need of customary, wired setup to reduce movement artifacts.

Experimental tests, performed in a wide spectrum of conditions, from slow to fast dynamic tasks, showed that the system can be easily worn and does not interfere with subject's movements. In all the tests, the device showed a high rejection of power line interference and movement artefacts. The measured low latency (12ms) between the transmitter and the receiver makes the device suitable for a wide range of real-time applications. Beside the clear advantages in terms of portability, the possibility of directly interfacing the HD-sEMG modules with a standard mobile device (e.g. Smartphone or Tablet) remove any constraints on the field of measure (usually limited by the maximum distance allowed between the transmitter and the receiver). The subject can wear and bring with him both the HD-sEMG modules and the mobile device that transmits the sampled data over the Internet. This approach opens possible applications in telemedicine, home rehabilitation, and training.

Overall, the characteristics of the proposed device (i) simplify the experimental setup; (ii) allow the detection of HD-sEMG in highly dynamic contractions; (iii) make the system usable in outdoor scenarios where high portability is required. Prospectively, this system may allow the exploitation of the

new possibilities offered by the recent development of stretchable electrodes and sensors. Whether this device could be deployed for the detection of bio-signals other than sEMG should be further investigated in future studies. For example, the overall architecture may be suitable for the detection of EEG signals, however, the choice of the analog front-end could be reconsidered in order to satisfy higher required performance in terms of signal to noise ratio.

Finally, the developed system has the potential to open new perspectives in the application of HD-sEMG technique in dynamic conditions and for the exploitation of this technique in clinical practice and in real-life applications.

ACKNOWLEDGMENT

The Authors thank Davide Mastrapasqua for the design of the Sensor Unit's plastic case and Phoenix PCB S.r.l. (Ivrea, Italy) for the support in PCBs production and mounting.

REFERENCES

[1] N. A. Dimitrova and G. V. Dimitrov, "Interpretation of EMG changes with fatigue: Facts, pitfalls, and fallacies," *J. Electromyogr. Kinesiol.*, vol. 13, no. 1, pp. 13–36, Feb. 2003.

[2] D. Farina, C. Cescon, and R. Merletti, "Influence of anatomical, physical, and detection-system parameters on surface EMG.," *Biol. Cybern.*, vol. 86, no. 6, pp. 445–56, 2002.

[3] D. Staudenmann, I. Kingma, A. Daffertshofer, D. F. Stegeman, and J. H. van Die??n, "Heterogeneity of muscle activation in relation to force direction: A multi-channel surface electromyography study on the triceps surae muscle," *J. Electromyogr. Kinesiol.*, vol. 19, no. 5, pp. 882–895, 2009.

[4] A. Gallina, R. Merletti, and M. Gazzoni, "Uneven spatial distribution of surface EMG: what does it mean?," *Eur. J. Appl. Physiol.*, vol. 113, no. 4, pp. 887–94, Apr. 2013.

[5] E. F. Hodson-Tole, I. D. Loram, and T. M. M. Vieira, "Myoelectric activity along human gastrocnemius medialis: Different spatial distributions of postural and electrically elicited surface potentials," *J. Electromyogr. Kinesiol.*, vol. 23, no. 1, pp. 43–50, 2013.

[6] A. Holtermann *et al.*, "Selective activation of neuromuscular compartments within the human trapezius muscle," *J. Electromyogr. Kinesiol.*, vol. 19, no. 5, pp. 896–902, 2009.

[7] K. Watanabe, M. Kouzaki, and T. Moritani, "Regional neuromuscular regulation within human rectus femoris muscle during gait in young and elderly men," *J. Biomech.*, vol. 49, no. 1, pp. 19–25, 2016.

[8] T. M. Vieira, A. Botter, S. Muceli, and D. Farina, "Specificity of surface EMG recordings for gastrocnemius during upright standing," *Sci. Rep.*, vol. 7, no. 1, 2017.

[9] K. Watanabe, M. Kouzaki, and T. Moritani, "Region-specific myoelectric manifestations of fatigue in human rectus femoris muscle," *Muscle and Nerve*, vol. 48, no. 2, pp. 226–234, 2013.

[10] R. Merletti, A. Botter, C. Cescon, M. A. Minetto, and T. M. M. Vieira, "Advances in Surface EMG: Recent Progress in Clinical Research Applications," *Crit. Rev. Biomed. Eng.*, vol. 38, no. 4, pp. 347–379, 2010.

[11] R. Merletti, M. Aventaggiato, A. Botter, A. Holobar, H. Marateb, and T. M. M. Vieira, "Advances in surface EMG: recent progress in detection and processing techniques.," *Crit. Rev. Biomed. Eng.*, vol. 38, no. 4, pp. 305–45, 2010.

[12] D. Farina, "Interpretation of the surface electromyogram in dynamic contractions," *Exercise and Sport Sciences Reviews*, vol. 34, no. 3. pp. 121–127, 2006.

[13] R. Merletti, D. Farina, and M. Gazzoni, "The linear electrode array: A useful tool with many applications," *J. Electromyogr. Kinesiol.*, vol. 13, no. 1, pp. 37–47, 2003.

[14] S. M. Wood, J. a Jarratt, a T. Barker, and S. H. M. Brown, "Surface electromyography using electrode arrays: a study of motor neuron disease.," *John Wiley - Muscle Nerve*, vol. 24, no. 2, pp. 223–30, 2001.

[15] S. Dick F., K. Bert U., L. Bernd G., and V. D. Johannes P., "High-density Surface EMG: Techniques and Applications at a Motor Unit Level," *Biocybern. Biomed. Eng.*, vol. 32, no. 3, pp. 3–27, 2012.

[16] B. G. Lapatki, J. P. Van Dijk, I. E. Jonas, M. J. Zwarts, and D. F. Stegeman, "A thin, flexible multielectrode grid for high-density surface EMG," *J. Appl. Physiol.*, vol. 96, no. 1, pp. 327–36, 2004.

[17] B. U. Kleine, J. P. van Dijk, B. G. Lapatki, M. J. Zwarts, and D. F. Stegeman, "Using two-dimensional spatial information in decomposition of surface EMG signals," *J. Electromyogr. Kinesiol.*, vol. 17, no. 5, pp. 535–548, 2007.

[18] B. U. Kleine, N. P. Schumann, D. F. Stegeman, and H. C. Scholle, "Surface EMG mapping of the human trapezius muscle: The topography of monopolar and bipolar surface EMG amplitude and spectrum parameters at varied forces and in fatigue," *Clin. Neurophysiol.*, vol. 111, no. 4, pp. 686–693, 2000.

[19] D. Prutchi, "A high-resolution large array (HRLA) surface EMG system," *Med. Eng. Phys.*, vol. 17, no. 6, pp. 442–454, 1995.

[20] T. Masuda, H. Miyano, and T. Sadoyama, "A surface electrode array for detecting action potential trains of single motor units," *Electroencephalogr. Clin. Neurophysiol.*, vol. 60, no. 5, pp. 435–443, 1985.

[21] M. Gazzoni, N. Celadon, D. Mastrapasqua, M. Paleari, V. Margaria, and P. Ariano, "Quantifying forearm muscle activity during wrist and finger movements by means of multi-channel electromyography," *PLoS One*, 2014.

[22] D. Farina, A. Holobar, R. Merletti, and R. M. Enoka, "Decoding the neural drive to muscles from the surface electromyogram," *Clinical Neurophysiology*, vol. 121, no. 10. pp. 1616–1623, 2010.

[23] M. Gazzoni, D. Farina, and R. Merletti, "A new method for the extraction and classification of single

motor unit action potentials from surface EMG signals," *J Neurosci Methods*, vol. 136, no. 2, pp. 165–177, 2004.

[24] V. Glaser, A. Holobar, and D. Zazula, "Real-time motor unit identification from high-density surface EMG," *IEEE Trans. Neural Syst. Rehabil. Eng.*, vol. 21, no. 6, pp. 949–958, 2013.

[25] A. A. Holobar and D. Zazula, "Multichannel blind source separation using convolution Kernel compensation," *IEEE Trans. Signal Process.*, vol. 55, no. 9, pp. 4487–4496, Sep. 2007.

[26] F. Negro, S. Muceli, A. M. Castronovo, A. Holobar, and D. Farina, "Multi-channel intramuscular and surface EMG decomposition by convolutive blind source separation," *J. Neural Eng.*, vol. 13, no. 2, 2016.

[27] D. Farina and A. Holobar, "Characterization of Human Motor Units from Surface EMG Decomposition," *Proc. IEEE*, vol. 104, no. 2, pp. 353–373, 2016.

[28] A. Botter and T. M. Vieira, "Optimization of surface electrodes location for H-reflex recordings in soleus muscle," *J. Electromyogr. Kinesiol.*, 2017.

[29] A. Gallina and T. Vieira, "Territory and fiber orientation of vastus medialis motor units: A Surface electromyography investigation," *Muscle and Nerve*, no. March, pp. 1057–1065, 2015.

[30] D. Farina *et al.*, "Principles of Motor Unit Physiology Evolve With Advances in Technology.," *Physiology (Bethesda).*, vol. 31, no. 2, pp. 83–94, 2016.

[31] E. Martinez-Valdes, C. M. Laine, D. Falla, F. Mayer, and D. Farina, "High-density surface electromyography provides reliable estimates of motor unit behavior," *Clin. Neurophysiol.*, vol. 127, no. 6, pp. 2534–2541, 2016.

[32] Karlatec D. and A. Holobar, "On Correlation Between the Neural Drive to Muscles and Multichannel Surface Electromyogram Amplitudes," in *Converging Clinical and Engineering Research on Neurorehabilitation II. Biosystems & Biorobotics*, 2017, pp. 1347–1351.

[33] C. v. d. Steeg, A. Daffertshofer, D. F. Stegeman, and T. W. Boonstra, "High-density surface electromyography improves the identification of oscillatory synaptic inputs to motoneurons," *J. Appl. Physiol.*, vol. 116, no. 10, pp. 1263–1271, 2014.

[34] B. G. Lapatki, J. P. Van Dijk, B. P. C. Van de Warrenburg, and M. J. Zwarts, "Botulinum toxin has an increased effect when targeted toward the muscle's endplate zone: A high-density surface EMG guided study," *Clin. Neurophysiol.*, vol. 122, no. 8, pp. 1611–1616, 2011.

[35] G. Drost, D. F. Stegeman, B. G. M. van Engelen, and M. J. Zwarts, "Clinical applications of high-density surface EMG: A systematic review," *J. Electromyogr. Kinesiol.*, vol. 16, no. 6, pp. 586–602, 2006.

[36] A. Gallina, S. Peters, J. L. Neva, L. A. Boyd, and S. J. Garland, "Selectivity of conventional electrodes for recording motor evoked potentials: An investigation with high-density surface electromyography," *Muscle and Nerve*, vol. 55, no. 6, pp. 828–834, 2017.

[37] B. Yao *et al.*, "Analysis of linear electrode array EMG for assessment of hemiparetic biceps brachii muscles," *Front. Hum. Neurosci.*, vol. 9, no. October, pp. 1–9, 2015.

[38] X. Zhang and P. Zhou, "High-density myoelectric pattern recognition toward improved stroke rehabilitation," *IEEE Trans. Biomed. Eng.*, vol. 59, no. 6, pp. 1649–1657, 2012.

[39] X. Li, A. Holobar, M. Gazzoni, R. Merletti, W. Z. Rymer, and P. Zhou, "Examination of poststroke alteration in motor unit firing behavior using high-density surface EMG decomposition," *IEEE Trans. Biomed. Eng.*, vol. 62, no. 5, pp. 1242–1252, 2015.

[40] G. van Elswijk, B. U. Kleine, S. Overeem, B. Eshuis, K. D. Hekkert, and D. F. Stegeman, "Muscle imaging: Mapping responses to transcranial magnetic stimulation with high-density surface electromyography," *Cortex*, vol. 44, no. 5, pp. 609–616, 2008.

[41] D. Farina and S. Amsüss, "Reflections On The Present And Future Of Upper Limb Prostheses," *Expert Rev. Med. Devices*, vol. 4440, no. May, p. 17434440.2016.1159511, 2016.

[42] W. Geng, Y. Du, W. Jin, W. Wei, Y. Hu, and J. Li, "Gesture recognition by instantaneous surface EMG images.," *Sci. Rep.*, vol. 6, no. October, p. 36571, 2016.

[43] H. Daley, K. Englehart, L. Hargrove, and U. Kuruganti, "High density electromyography data of normally limbed and transradial amputee subjects for multifunction prosthetic control," *J. Electromyogr. Kinesiol.*, vol. 22, no. 3, pp. 478–484, 2012.

[44] N. Jiang, J. L. Vest-Nielsen, S. Muceli, and D. Farina, "EMG-based simultaneous and proportional estimation of wrist/hand dynamics in uni-Lateral trans-radial amputees," *J. Neuroeng. Rehabil.*, vol. 9, no. 1, p. 42, 2012.

[45] D. C. Tkach, A. J. Young, L. H. Smith, E. J. Rouse, and L. J. Hargrove, "Real-time and offline performance of pattern recognition myoelectric control using a generic electrode grid with targeted muscle reinnervation patients," *IEEE Trans. Neural Syst. Rehabil. Eng.*, vol. 22, no. 4, pp. 727–734, 2014.

[46] D. Farina *et al.*, "The extraction of neural information from the surface EMG for the control of upper-limb prostheses: Emerging avenues and challenges," *IEEE Trans. Neural Syst. Rehabil. Eng.*, vol. 22, no. 4, pp. 797–809, 2014.

[47] M. Pozzo, A. Bottin, R. Ferrabone, and R. Merletti, "Sixty-four channel wearable acquisition system for long-term surface electromyogram recording with electrode arrays," *Med. Biol. Eng. Comput.*, vol. 42, no. 4, pp. 455–466, 2004.

[48] U. Barone and R. Merletti, "Design of a portable, intrinsically safe multichannel acquisition system for high-resolution, real-time processing HD-sEMG," *IEEE Trans. Biomed. Eng.*, vol. 60, no. 8, pp. 2242–2252, 2013.

[49] R. R. Harrison and C. Charles, "A low-power low-noise CMOS amplifier for neural recording

applications," *IEEE J. Solid-State Circuits*, vol. 38, no. 6, pp. 958–965, 2003.

[50] R. R. Harrison *et al.*, "A low-power integrated circuit for a wireless 100-electrode neural recording system," *IEEE J. Solid-State Circuits*, vol. 42, no. 1, pp. 123–133, 2007.

[51] A. C. Metting van Rijn, A. Peper, and C. A. Grimbergen, "High-quality recording of bioelectric events - Part 1 Interference reduction, theory and practice," *Medical & Biological Engineering & Computing*. 1990.

[52] B. B. Winter and J. G. Webster, "Reductionl of Interference Due to Common Mode Voltage in Biopotential Amplifiers," *IEEE Trans. Biomed. Eng.*, 1983.

[53] E. M. Spinelli, M. A. Mayosky, and R. Pallás-Areny, "A practical approach to electrode-skin impedance unbalance measurement," *IEEE Trans. Biomed. Eng.*, 2006.

[54] G. Piervirgili, F. Petracca, and R. Merletti, "A new method to assess skin treatments for lowering the impedance and noise of individual gelled Ag-AgCl electrodes," *Physiol. Meas.*, 2014.

[55] J. C. Huhta and J. G. Webster, "60-Hz Interference in Electrocardiography," *IEEE Trans. Biomed. Eng.*, 1973.

[56] A. Gallina, C. H. Ritzel, R. Merletti, and T. M. M. Vieira, "Do surface electromyograms provide physiological estimates of conduction velocity from the medial gastrocnemius muscle?," *J. Electromyogr. Kinesiol.*, 2013.

[57] B. Afsharipour, F. Petracca, M. Gasparini, and R. Merletti, "Spatial distribution of surface EMG on trapezius and lumbar muscles of violin and cello players in single note playing," *J. Electromyogr. Kinesiol.*, vol. 31, pp. 144–153, 2016.

[58] J. G. Webster, "Reducing motion artifacts and interference in biopotential recording.," *IEEE Trans. Biomed. Eng.*, vol. 31, no. 12, pp. 823–826, 1984.

[59] J. A. J. Klijn and M. J. G. M. Kloprogge, "Movement artefact suppressor during ECG monitoring," *Cardiovasc. Res.*, vol. 8, no. 1, pp. 149–152, 1974.

[60] H. W. Tam and J. G. Webster, "Minimizing Electrode Motion Artifact by Skin Abrasion," *IEEE Trans. Biomed. Eng.*, vol. BME-24, no. 2, pp. 134–139, 1977.

[61] R. Gatzke, "The electrode: a measurement systems viewpoint," in *Biomedical electrode technology*, 1974, p. 447.